Seasonality and drought effects of Amazonian forests observed from multi-angle satellite data

Citation	de Moura, Y. M., Hilker, T., Lyapustin, A. I., Galvão, L. S., dos Santos, J. R., Anderson, L. O., ... & Arai, E. (2015). Seasonality and drought effects of Amazonian forests observed from multi-angle satellite data. Remote Sensing of Environment, 171, 278-290. doi:10.1016/j.rse.2015.10.015
DOI	10.1016/j.rse.2015.10.015
Publisher	Elsevier
Version	Version of Record
Terms of Use	http://cdss.library.oregonstate.edu/sa-termsofuse

Remote Sensing of Environment 171 (2015) 278–290

Contents lists available at ScienceDirect

Remote Sensing of Environment

journal homepage: www.elsevier.com/locate/rse

Seasonality and drought effects of Amazonian forests observed from multi-angle satellite data

Yhasmin Mendes de Moura [a,*], Thomas Hilker [b], Alexei I. Lyapustin [c], Lênio Soares Galvão [a], João Roberto dos Santos [a], Liana O. Anderson [d,e], Célio Helder Resende de Sousa [b], Egidio Arai [a]

[a] National Institute for Space Research (INPE), Avenida dos Astronautas, 1758 São José dos Campos, SP, Brazil
[b] Oregon State University, College of Forestry, Corvallis, OR 97331, USA
[c] NASA Goddard Space Flight Center, Greenbelt, MD 20771, USA
[d] National Centre for Monitoring and Early Warning of Natural Disasters (CEMADEN), Estrada Doutor Altino Bondensan, 500, São José dos Campos, SP, Brazil
[e] Environmental Change Institute, University of Oxford, Oxford OX1 3QY, UK

ARTICLE INFO

Article history:
Received 25 March 2015
Received in revised form 9 October 2015
Accepted 22 October 2015
Available online 5 November 2015

Keywords:
Amazon
Drought
Anisotropy
Greening
Browning
MAIAC
MODIS

ABSTRACT

Seasonality and drought in Amazon rainforests have been controversially discussed in the literature, partially due to a limited ability of current remote sensing techniques to detect its impacts on tropical vegetation. We use a multi-angle remote sensing approach to determine changes in vegetation structure from differences in directional scattering (anisotropy) observed by the Moderate Resolution Imaging Spectroradiometer (MODIS) with data atmospherically corrected by the Multi-Angle Implementation Atmospheric Correction Algorithm (MAIAC). Our results show a strong linear relationship between anisotropy and field ($r^2 = 0.70$) and LiDAR ($r^2 = 0.88$) based estimates of LAI even in dense canopies (LAI ≤ 7 m^2 m^{-2}). This allowed us to obtain improved estimates of vegetation structure from optical remote sensing. We used anisotropy to analyze Amazon seasonality based on spatially explicit estimates of onset and length of dry season obtained from the Tropical Rainfall Measurement Mission (TRMM). An increase in vegetation greening was observed during the beginning of dry season (across ~7% of the basin), which was followed by a decline (browning) later during the dry season (across ~5% of the basin). Anomalies in vegetation browning were particularly strong during the 2005 and 2010 drought years (~10% of the basin). We show that the magnitude of seasonal changes can be significantly affected by regional differences in onset and duration of the dry season. Seasonal changes were much less pronounced when assuming a fixed dry season from June through September across the Amazon Basin. Our findings reconcile remote sensing studies with field based observations and model results as they provide a sounder basis for the argument that tropical vegetation growth increases during the beginning of the dry season, but declines after extended drought periods. The multi-angle approach used in this work may help quantify drought tolerance and seasonality in the Amazonian forests.

1. Introduction

Vulnerability of tropical forests to climate change has received broad attention by the scientific community as increase in equatorial sea surface temperature (SST) can lead to longer dry seasons (Fu et al., 2013; Marengo, Tomasella, Alves, Soares, & Rodriguez, 2011) and more frequent, severe drought events (Lewis, Brando, Phillips, van der Heijden, & Nepstad, 2011; Malhi, Aragão, Galbraith, et al., 2009; Malhi, Aragão, Metcalfe, et al., 2009; Marengo et al., 2008). The feedbacks of such drying on global climate change could be substantial; the Amazon rainforest alone accounts for about 15% of global photosynthesis and hosts perhaps a quarter of the world's terrestrial species (Malhi et al., 2008). Field studies have indicated that such extreme drought events could alter species composition, biodiversity (Asner & Alencar, 2010; Asner, Nepstad, Cardinot, & Ray, 2004, April 20; Phillips et al., 2009) and plant productivity (Aragao et al., 2007; Gatti et al., 2014; Meir, Metcalfe, Costa, & Fisher, 2008).

Over the last decade, the Amazon region has experienced two severe droughts, one in 2005 and another in 2010 (Marengo et al., 2011). However, the broad scale response of vegetation to these events remains controversial. Saleska, Didan, Huete, and da Rocha (2007) reported an increase in greenness (higher EVI) for the 2005 drought, a result that was subsequently challenged (Atkinson, Dash, & Jeganathan, 2011; Samanta et al., 2010). Xu et al. (2011) observed a widespread decline in greening for the 2010 drought. Similarly, the prevailing view of seasonality of vegetation has recently been discussed. Several findings (Brando et al., 2010; Graham, Mulkey, Kitajima, Phillips, & Wright, 2003; Huete et al., 2006; Hutyra et al., 2007; Myneni et al., 2007; Samanta et al., 2012; Wagner, Rossi, Stahl, Bonal, & Hérault, 2013)

* Corresponding author.
E-mail address: yhas.mendes@gmail.com (Y.M. de Moura).

http://dx.doi.org/10.1016/j.rse.2015.10.015
0034-4257/

support the view that photosynthetic activity increases initially during the dry season in response to an increase in incident photosynthetically active radiation (PAR). However, a recent study based on NASA's Moderate Resolution Imaging Spectroradiometer (MODIS) (Morton et al., 2014) argued that seasonal changes are driven by artifacts of the sun-sensor geometry.

A growing body of literature suggests uncertainties in remote sensing of atmospheric aerosol loadings (Samanta et al., 2010, 2012) and deficiencies in cloud detection (Hilker et al., 2012) to be partially responsible for these contradicting results. While progress has been made addressing some of these challenges by using alternative datasets (Hilker et al., 2014) or higher spatial resolution imagery (Zelazowski, Sayer, Thomas, & Grainger, 2011), observations based on remotely sensed vegetation indices are limited in their ability to detect changes in vegetation cover due to a well-documented saturation effect in areas with high biomass and leaf area (Carlson & Ripley, 1997).

As an alternative to observations from only one view angle, the combination of multiple view angles may provide new opportunities to mitigate these saturation effects, and allow better insights into seasonal and inter-annual changes of tropical forests. Biophysical changes in the canopy structure affect the directional scattering of light and these effects are observable from multi-angular data (Chen, Menges, & Leblanc, 2005). With the advance of multi-angular sensors such as the Multi-angle Imaging SpectroRadiometer (MISR) (Diner et al., 1998), progress has been made in describing the dependence of reflectance on observation angles (Barnsley, Settle, Cutter, Lobb, & Teston, 2004; Diner et al., 1998). For instance, the angular component of surface reflectance (anisotropy) has been linked to optical properties and geometric structure of the target (Widlowski et al., 2004; Widlowski, Pinty, Lavergne, Verstraete, & Gobron, 2005) such as canopy roughness (Strahler, 2009), leaf angle distribution (Roujean, 2002), leaf area index (LAI) (Walthall, 1997) and foliage clumping (Chen et al., 2005).

The theoretical basis for the influence of canopy structure on multi-angle reflectance has been developed (Bicheron, 1999; Chen, Liu, Leblanc, Lacaze, & Roujean, 2003; Gao, 2003; Leblanc et al., 2005; Myneni et al., 2002). However, multi-angle reflectance is not easily obtained from traditional surface reflectance algorithms, even when data is acquired from multiple view angles. Pixel based algorithms often assume a Lambertian reflectance model, which reduces the anisotropy of the derived surface reflectance (Lyapustin & Muldashev, 1999; Wang et al., 2010) thus decreasing the ability to detect directional scattering (Hilker et al., 2009).

New methods for processing remote sensing data, such as the Multi-Angle Implementation of Atmospheric Correction (MAIAC), can help overcome this limitation by using a radiative transfer model that does not make a Lambertian assumption (Lyapustin & Knyazikhin, 2001). MAIAC is a cloud screening and atmospheric correction algorithm that uses an adaptive time series analysis and processing of groups of pixels to derive atmospheric aerosol concentration and surface reflectance. A detailed description of the algorithm can be found in Lyapustin et al. (2011), Lyapustin, Wang, Laszlo, Hilker, et al., (2012). In this paper, we take advantage of MAIAC to study changes in anisotropy across the Amazon Basin using thirteen years of multi-angle MODIS observations. We define anisotropy as difference in reflectance between the backscattering (relative azimuth angle (RAA) = 180°) and the forward scattering (RAA = 0°) directions for a fixed view and sun zenith angle. Estimates of such defined anisotropy were then related to field and LiDAR-based estimates of LAI in order to validate its relation to vegetation structure. Our objectives were to demonstrate spatial and temporal changes in anisotropy, particularly during the onset of the dry season as a measure of changes in vegetation. We re-visited the two last major droughts in the Amazon Basin (2005 and 2010) to evaluate anomalies in anisotropy and investigate vegetation response to these drought events on a monthly basis.

2. Material and methods

2.1. Quantification of multi-angle scattering

MAIAC data were obtained from 12 MODIS tiles (h10v08 to h13v10, spanning 10° N to 20° S in latitude and 80° W to 42° W in longitude) from Terra and Aqua satellites between 2000 and 2012. MAIAC is based on MODIS Level 1B (calibrated and geometrically corrected) observations, which remove major sensor calibration degradation effects present in earlier collections (Lyapustin et al., 2014). MAIAC grids MODIS L1B data to a 1 km resolution, and accumulates measurements of the same surface area from different orbits (view geometries) for up to 16 days using a moving window approach. These data are used to derive spectral regression coefficients relating surface reflectance in the blue (0.466 μm) and shortwave infrared (2.13 μm) for aerosol retrievals, and to obtain parameters of surface bi-directional reflectance distribution function (BRDF) (Lyapustin et al., 2011; Lyapustin, Wang, Laszlo, Hilker, et al., 2012). Assuming that vegetation is relatively stable during this period, the surface directional scattering can be characterized using the Ross-Thick Li-Sparse (RTLS) BRDF model (Roujean, Leroy, & Deschamps, 1992). During periods of rapid surface change (e.g., green-up or senescence) MAIAC follows an approach of the MODIS BRDF/albedo algorithm (MOD43, Schaaf et al., 2002) to scale the BRDF model with the latest measurement to adjust the magnitude of reflectance while assuming that the shape of BRDF does not change significantly. This approach preserves spectral contrasts of actual surface characteristics.

One advantage of using the RTLS model rather than reflectance directly is the possibility to maintain constant sun-observer geometry and extrapolate measurements to the principal plane to describe backscatter and forward scatter directions. In this study, we selected a view zenith angle (VZA) of 35° rather than the absolute hotspot location at VZA = 45° in order to keep the modeled reflectance closer to the actual range of angles observed by MODIS, thereby minimizing potential errors resulting from extrapolation of the BRDF. For land vegetated surfaces, directional scattering dominates in the NIR region due to the high absorption of visible light. Rather than obtaining anisotropy of the NIR band alone, we calculated forward and backscatter for blue, red and NIR reflectance and then obtained the Enhanced Vegetation Index (three-band version EVI) for both directions. The objective of using EVI rather than surface reflectance of a given band was to minimize the effect of non-photosynthetically active elements while optimizing the sensitivity to green canopy structure. It can, however, be shown that differences between forward and backward scatter EVI is largely the result of differences in scattering in the near infrared region (Moura, Galvão, dos Santos, Roberts, & Breunig, 2012).

The spectral error of MAIAC surface reflectance was evaluated as the standard deviation between observed surface reflectance (BRF) and BRDF model prediction 1) over a time (using an area of 100 × 100 km to obtain sufficient statistics given high cloud cover in Amazonia) and 2) in space (pixel by pixel) for the example of two 30 day periods, in June and September.

2.2. LiDAR based estimates of leaf area index

Estimates of anisotropy were validated against existing and independent field observations of LAI ($n = 16$) obtained from the literature (Andreae, 2002; Figuera et al., 2011; Domingues, Berry, Martinelli, Ometto, & Ehleringer, 2005; Doughty & Goulden, 2000a,b; Galvao et al., 2011; Malhi, Aragão, Galbraith, et al., 2009; Malhi, Aragão, Metcalfe, et al., 2009; Negrón Juárez, da Rocha, Figueira, Goulden, & Miller, 2009;Restrepo-Coupe et al., 2013; Scurlock, Asner, & Gower, 2001; Zanchi et al., 2009), and Airborne Laser Scanning (ALS) as an example of a measure of canopy structure. LiDAR data were acquired by the Sustainable Landscapes Brazil project supported by the Brazilian Agricultural Research Corporation (EMBRAPA), the US Forest Service, USAID, and the

US Department of State. A detailed description of the LiDAR data can be found at http://mapas.cnpm.embrapa.br/paisagenssustentaveis. In order to allow a comparison between LiDAR based LAI and anisotropy, the area of airborne LiDAR acquisition was first subdivided into 1 × 1 km tiles matching the MODIS pixels. The probability of canopy gap within each tile was then determined as the sum of the total number of hits down to a height z, relative to the total number of independent LiDAR shots (N) (Lovell, Jupp, Culvenor, & Coops, 2003; Reading, Bedunah, & Amgalanbaatar, 2006):

$$P_{gap}(z) = \frac{1 - \sum_{z=j}^{z=z_{max}} \#z_j}{N} \quad (1)$$

where #z is the number of hits down to a height z above the ground (or the range to which the gap probability is taken). Finally, the leaf area profile L(z) was modeled as a logarithmic function of P_{gap} (Lovell et al., 2003) assuming an exponential extinction of light within the canopy:

$$L(z) = -\log(P_{gap}(z)). \quad (2)$$

A detailed description of the method applied can be found in (Coops et al., 2007).

2.3. Estimating onset and duration of Amazon dry seasons

The most common period used in the literature for describing dry seasons across Amazonia is June through September (Saleska et al., 2007; Samanta et al., 2010; Xu et al., 2011). It is, however, widely acknowledged that the actual onset and duration of the dry season varies greatly across the Amazon Basin (Silva et al., 2013). In order to investigate the effects of regional variability in precipitation, onset and length of dry season were calculated for each year using monthly estimates of water deficit from precipitation obtained from Tropical Rainfall Measuring Mission (TRMM) (3B43 v7 and 7A, at 0.25° spatial resolution). TRMM data has been extensively used to characterize the seasonal and inter-annual variability in rainfall across the Amazon region (Aragao et al., 2007). Dry season months were determined by using the assumption that moist tropical forests transpire about 100 mm·month^{-1} (Anderson, 2012; Aragao et al., 2007): When rainfall drops below 100 mm·month^{-1}, evapotranspiration exceeds precipitation, and soil water availability declines (Borchert, 1998; A. Strahler & D. Jupp, 1990; Williams et al., 1998).

3. Results

The left column in Fig. 1 shows an example of a BRDF surface fitted to retrieve forward and backscatter for red reflectance (a) and NIR reflectance (c). We also illustrated a BRDF surface calculated for EVI (e) to demonstrate the anisotropy of this index. The RTLS surfaces are shown for a 1 × 1 km area of Amazon forest (65°0′0″ W, 5°0′0″ S) using all observations acquired between January 1 and 14, 2006. The polar coordinates represent the view zenith and azimuth angles, the z-axis shows the corresponding reflectance (ρ) in the red and NIR bands, and EVI, respectively. The black dots represent the MODIS observations that were used to parameterize the BRDF surface. The red and blue dots show the modeled forward and backscatter reflectance (Fig. 1, left column) with a fixed sun observer geometry (SZA = 45°, VZA = 35°, RAA = 180° in the backscatter direction and SZA = 45°, VZA = 35°, RAA = 0° in the forward scatter direction). We fitted one such surface for each pixel and 14-day period to derive bi-weekly anisotropy across the Amazon Basin.

Fig. 1b, d and f show temporal variations in anisotropy (for red, NIR and EVI, respectively) for different sun observer geometries to verify the robustness of the method applied. The time series shows a spatial average of MODIS tile h12v09 (south-central Amazon) as an example. We varied the solar zenith angle between 45° (which is the default angle for BRDF normalization in MAIAC) and 25° degrees (which is more commonly found in tropical latitudes). Results shows strong seasonal variations for red and NIR reflectance (variations in the blue band are not shown), and resulting EVI, irrespective of the modeled SZA. While reflectance and EVI anisotropy increased with increasing SZA, the seasonal difference remained similar. The seasonal robustness with respect to a given SZA may be explained by the fact that the region around hotspot and darkspot area is relatively smooth (Fig. 1a, c and e), making estimates of seasonal anisotropy relatively insensitive to the particular sun-sensor configuration selected, as long as this configuration remains constant.

Figs. A.2 and A.3 provide a quantitative analysis of the standard deviation (σ) between observed surface reflectance and BRDF model prediction. Fig. A.2 shows the behavior of the standard deviation over a time, using an area of 100 × 100 km area as an example (65°0′0″ W, 5°0′0″ S). The mean standard deviations were 0.005 and 0.019 for the red and NIR reflectance, respectively, which is about 10–15% of the seasonal changes illustrated in Fig. 1a and b. Slight seasonal variability in σ was found, likely as a result of increased cloud cover during the wet season. Fig. A.3 illustrates the spatial variability of the standard deviation in June (Fig. A.3a) and September (Fig. A.3b). For reasons of brevity only the variability in EVI is presented. Similar to Fig. A.2, the standard deviation between observed EVI and model prediction presented in Fig. A.3 was on average about 5–10% of the observed seasonal changes (compare Fig. 1).

Fig. 2 illustrates the spatio-temporal variation in anisotropy by means of its first principal component (PC1) for the period between 2000 and 2012. The droughts years 2005 and 2010 were excluded from this analysis to only represent normal year variations. PC1 explained about 89% of the total variance in anisotropy; consequently, we focus on this first component to illustrate regional variability in the dataset. Red and yellow represent areas with relatively higher anisotropy, while green to white show areas with relatively lower anisotropy. Notable differences were found not only between the Amazonian rainforest and non-forested savannah regions, but also within the forested area itself (compare traditional vegetation indices for instance in Hilker et al., 2014, Fig. S2). High anisotropy was found predominantly in the more densely forested areas in northern and eastern Amazonia whereas the open forest types in the southern regions yielded, on average, lower values of anisotropy. The point symbols in Fig. 2 illustrate the plot locations for field based observations of LAI and LiDAR derived measurements. While the total number of independent LAI estimates is limited across remote forested areas such as the Amazon Basin, the field locations indicated in Fig. 2 represented a reasonable range of forest types within the Amazon rainforest.

Measures of anisotropy were strongly related to independent field observations of LAI ($n = 16$) obtained from the literature (Fig. 3a, $r^2 = 0.70$ $p < 0.05$) and LAI estimates derived from airborne LiDAR (Fig. 3b, $r^2 = 0.88$ $p < 0.05$). Importantly, both relationships were found to be linear, at least within the observed range of LAI ≤ 7 m^2 m^{-2} and yielded an improved description of structure in densely vegetated areas compared to estimates obtainable from nadir EVI images alone (Fig. 3c). The relationship between both field measured and LiDAR LAI estimates with anisotropy followed almost the identical linear functional form, which allowed us to describe leaf area across a range of vegetation types within the Amazonian rainforest from both data sources.

In addition to a large heterogeneity in vegetation structure (Fig. 2), our analysis confirmed also a large variability in precipitation across the basin (Villar et al., 2009). Fig. 4 represents estimates of monthly water deficit. Areas with low water deficit are shown in blue, whereas red indicates high water deficits. Areas with no water deficit are presented without color. High levels of water deficit were found in the northern Amazon region mainly between January and March, corresponding to the dry season in the northern hemisphere, whereas May

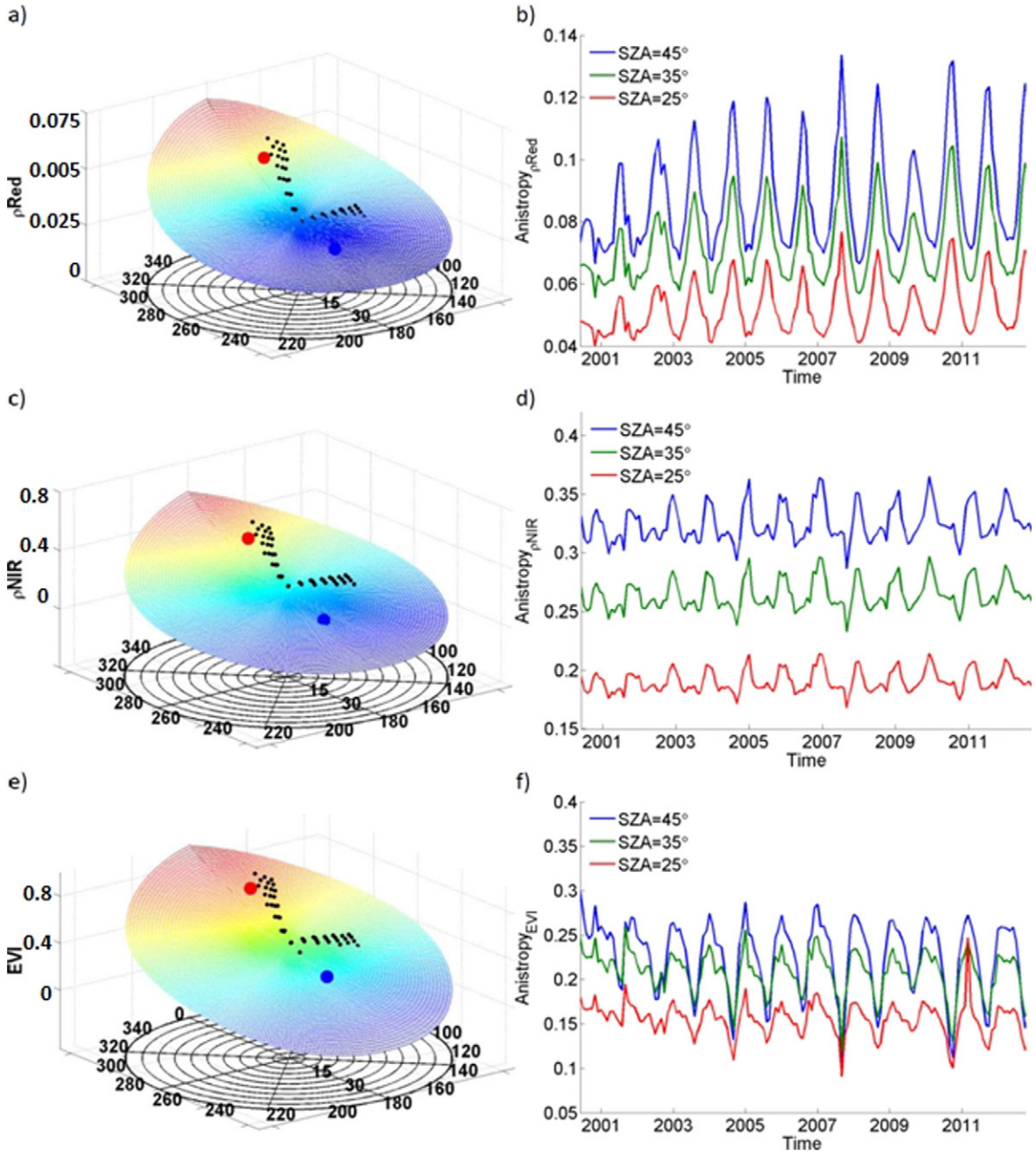

Fig. 1. Modeled BRDF surface for a 1 × 1 km area of Amazon forest (65°0′0″ W, 5°0′0″ S) for red reflectance (a), NIR reflectance (c) and EVI (e). The black dots represent the actual MODIS observations accumulated over a 14 day period, the blue dot represents the modeled forward scatter direction (darkspot), the red dot represents the modeled backscatter direction (hotspot). Fig. 1b, d and f show a time series of anisotropy (red, NIR and EVI, respectively) using the mean time series of MODIS tile h12v09. Sun. zenith angles (SZA) varied between 45° and 25° degrees to investigate the sensitivity with respect to the sun sensor configuration.

to August marked the dry season months across large parts of the southern hemisphere. Overall, the largest water deficit was found during June and July (focusing on the south-eastern border of the Amazon), whereas the lowest levels of water deficit were observed during March, with precipitation exceeding 100 mm month^{-1} almost across the entire basin. The beginning and length of dry season (Fig. 5a and b, respectively) varied accordingly and followed a south-west north-east gradient with up to 5 months of water deficit in the south-west. By contrast, large areas of Amazonas state, central Amazon, showed, on average, no water deficit during the observed years (gray area in the map, compare also Steege & Pitman, 2003).

Anisotropy changes in response to these seasonal variations in precipitation are shown in Fig. 6. Fig. 6a and b show total differences in anisotropy between beginning and end of the dry season (positive changes are labelled "greening", negative changes are labeled "browning"; all changes are normalized with respect to their standard deviations). Absolute changes (non-normalized) in anisotropy at beginning and end of dry season are presented in A.1. Only those changes that exceeded the RMSE of the field validation (Fig. 3a and b) are presented. Non-forested areas were excluded from all analysis using the MODIS land cover product (collection 5, Friedl et al., 2010). Fig. 6a uses a fixed dry season assumption from June through September to derive conventional measures of greening/browning. Fig. 6b shows changes of greening/browning based on onset and length of dry season derived from water deficit. In both cases, the drought years of 2005 and 2010 were excluded from the analyses to reflect "normal year" situations. In case of the fixed dry season assumption (Fig. 6a), negative net changes in anisotropy were found largely in the west and north-western region

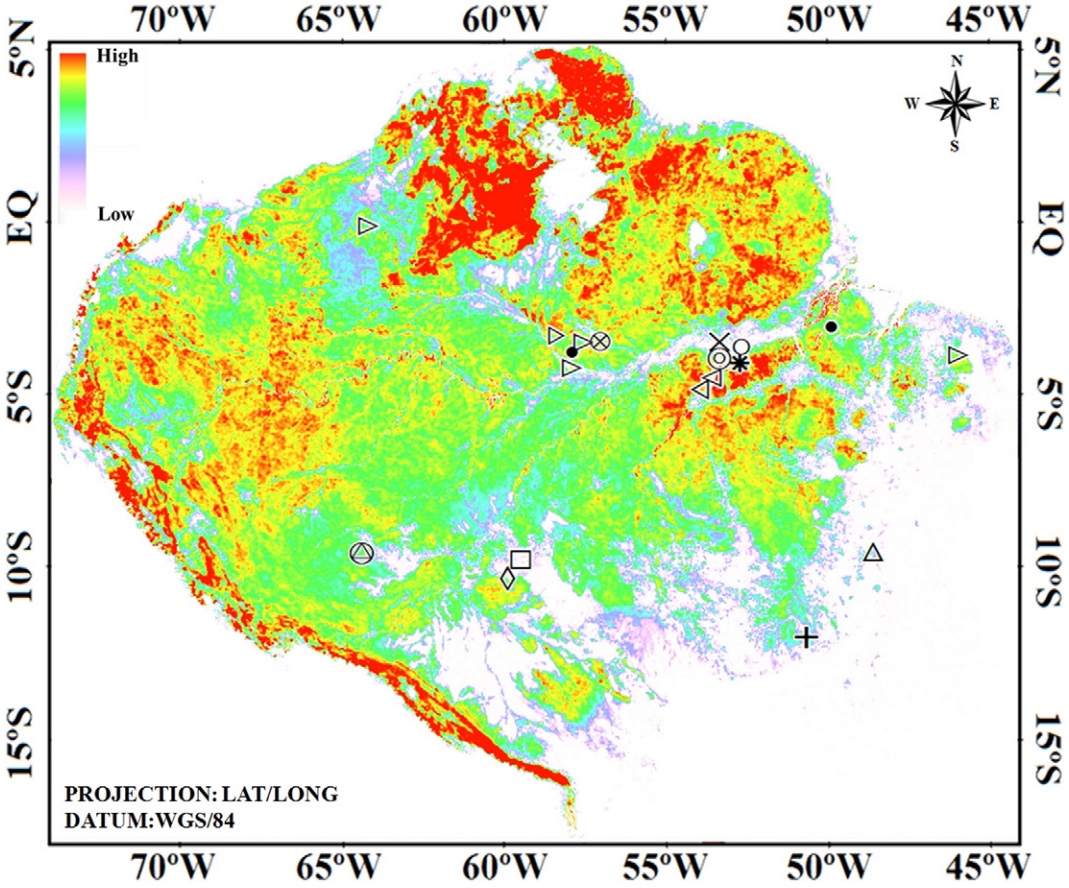

Fig. 2. The first principal component of anisotropy between 2000 and 2012. The droughts years 2005 and 2010 were excluded. The locations of the field and LiDAR estimates of LAI are shown. LiDAR estimates were obtained from Sustainable Landscape Project in three locations: Adolpho Ducke Forest Reserve, Amazonas state, Brazil (⊗); Rio Branco municipality, Acre State, Brazil (⏀) and Tapajós National Forest, Pará State, Brazil (◎). The other field estimates of LAI were collected from the literature: Malhi, Aragão, Galbraith, et al. (2009), Malhi, Aragão, Metcalfe, et al. (2009) (•), Domingues et al. (2005) (○), Doughty and Goulden (2008c) (*), Negrón Juárez et al. (2009) (x), Andreae et al. (2002) (□), Zanchi et al. (2009) (◇), Restrepo-Coupe et al. (2013) (Δ), Figuera et al. (2011) (<), Scurlock et al. (2001) (˚), Galvao et al. (2011) (+).

of the Amazon Basin, while small greening effects were observed in the Amapá state region and south-central Amazonia. When considering the specific length of dry season (Fig. 6b), it becomes apparent that most of the area showing net browning effects did actually not experience a seasonal water deficit (Fig. 6a), at least on average within the time period observed. Net greening effects shown in Fig. 6b were similar to those presented in Fig. 6a. However, regionally, considerable differences were found, particularly in the south western part of the study area. Compared to the normalized results, non-normalized differences in anisotropy between the beginning and end of dry season were prominent across most of the Amazon Basin (A.1), which can be explained by the relatively small RMSE obtained from the validation dataset (Fig. 3a and b).

Fig. 6c and d show net greening and browning effects in percentage of total area per month of dry season. Greening and browning effects were defined as percentage of pixels with significant increase/decrease in anisotropy ($\geq 2\sigma$) compared to the annual mean. Fig. 6c uses a fixed dry season assumption (June through September), while Fig. 6d shows changes based on onset of dry season derived from water deficit. In case of Fig. 6d, we also show the last month before a water deficit was observed, in order to illustrate changes in photosynthetic activity with the reduction of rainfall towards the end of the rainy season. Both estimates showed increased anisotropy during the beginning of the dry season with about 2% of area experiencing "greening" when using a fixed dry season assumption and over 5% of total area greening when explicitly considering dry season onset for each pixel. In both analyses, greening effects turned into net browning effects after an extended length of dry season, reaching about 7% of the area after 3 or more months when accounting for actual dry season onset. Monthly changes in LAI (as deviations from annual means) were calculated using the linear relationships to field and LiDAR measurements presented in Fig. 3. The dashed line in Fig. 6c and d represent estimates based on the relationship with field observations (Fig. 3a), while the solid line represents estimates based on the relationship with LiDAR observations (Fig. 3b). Consistent with the net changes in area of greening and browning, our results suggested that total leaf area increases during the beginning of the dry season by on average 0.2 $m^2\ m^{-2}$ across the basin, while LAI dropped below the annual mean after about 2 months of dry season (0.1 $m^2\ m^{-2}$). However, these results should be interpreted carefully as changes in LAI varied greatly across space and may also be the result of changes in other structural parameters (see discussion).

The two drought years resulted in strong browning effects; spatial and temporal patterns of anomalies in anisotropy for the 2005 and 2010 droughts are presented in Fig. 7. For both years, only the specific beginning and end of the dry season (based on the water deficit) are shown. Fig. 7 shows *anomalies* i.e. deviations from the normal year patterns presented in Fig. 6; all anomalies were normalized to the standard deviation ($\geq 2\sigma$) of the years 2000–2012, excluding 2005 and 2010. While positive and negative anomalies were approximately balanced at the beginning of the dry season (Fig. 7c and d), negative anomalies in anisotropy outweighed positive effects after about three months, especially during 2010, with negative anomalies being three times larger than positive ones. Estimates of derived LAI showed small positive anomalies during the beginning of the 2005 drought period, but confirmed large negative effects with extended dry season length. In 2010, change was similar to normal years (anomalies were

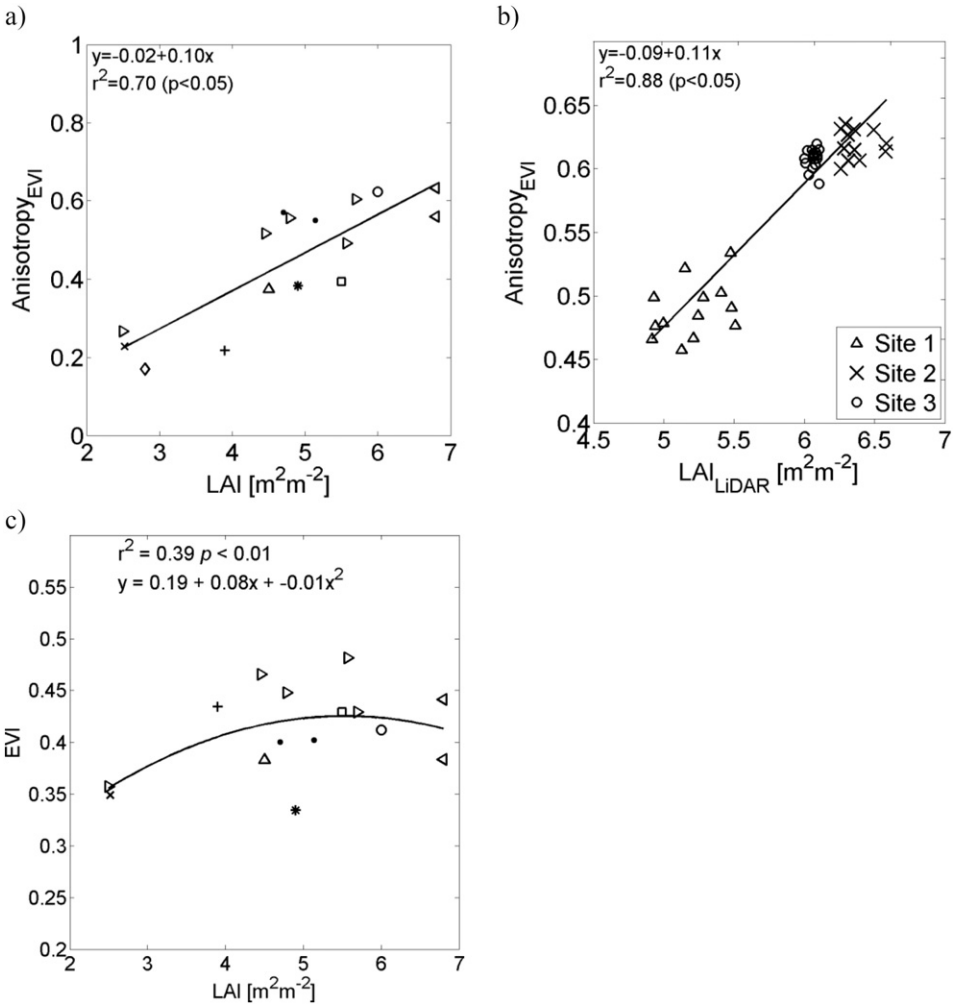

Fig. 3. Relationship between anisotropy and LAI; a) from field values collected in the literature (see Fig. 2), and b) from LiDAR estimates. c) Relationship between directionally normalized (nadir) EVI and LAI. The correlations were performed using the dates described in the field data with the closest MODIS acquisitions available. The location of the plots are provided in Fig. 2. RMSE for Fig. 3a and b were 0.08 and 0.02 (units of anisotropy), respectively.

small) during the first few months of the dry season. However, areas with 6 months of dry season showed negative deviation from normal year decline in structure (Fig. 6d) of an additional $-0.2\ m^2\ m^{-2}$ across the basin (Fig. 7d).

4. Discussion

This study used multi-angle observations from the MODIS instrument to investigate spatial and temporal variability in vegetation structure across the Amazon Basin. While the range of view angles acquired from MODIS is relatively small (Fig. 1), as the instrument was not specifically designed for multi-angle acquisitions, anisotropy still provided an effective means to characterize vegetation structure across the Amazon forest. Changes in the sun-sensor configuration over the year do not always allow to model forward and backscattering observations within the sampling range of the MODIS instruments. However, the analysis presented in Fig. 1 has demonstrated a relative robustness with respect to the selected sun-sensor configuration. The standard deviation between observed and modeled MAIAC reflectance (Figs. A.2 and A.3) was about 10% of the observed variation in anisotropy (Figs. 6 and 7), confirming the ability of our approach to detect seasonal and interannual changes. The results were further within the range of the RMSE reported in Fig. 3, thereby confirming the significance of the relationship to canopy structure. The approach should account for error sources from undetected clouds to gridding uncertainties. It should further account for limitations of the RTLS model to describe the BRDF shape and anisotropy of the MAIAC data.

Our results suggest that structural information of vegetation may be obtained frequently over large areas from MODIS. Further research, however, will be needed to investigate potentials for other ecosystems and regions. The BRDF model selected in this study allowed us to derive seasonal anisotropy independent of the sun observer geometry, which is an important consideration for separating vegetation seasonality from artifacts due to seasonal changes in the sun/sensor constellation (Morton et al., 2014).

While it is acknowledged that vegetation may change over a 14 day period, as used in our BRDF approach, this technique should still allow us to observe most seasonality of vegetation and has proven useful in other composite products (Huete et al., 2002; Schaaf et al., 2002). Data scarcity may prevent frequent updates of BRDF shapes, which in some cases limit the ability to determine anisotropy and may lead to misinterpretation of changes in canopy structure. However, analysis of observation frequency across the Amazon Basin (Hilker et al., 2015) has shown that MAIAC provides on average between 10 and 60 observations in any given month from Terra and Aqua, respectively, which should allow stable BRDF inversions for most pixels. Other methods to derive multidirectional reflectance (Franch, Vermote, Sobrino, & Fédèle, 2013; Schaaf et al., 2002) have

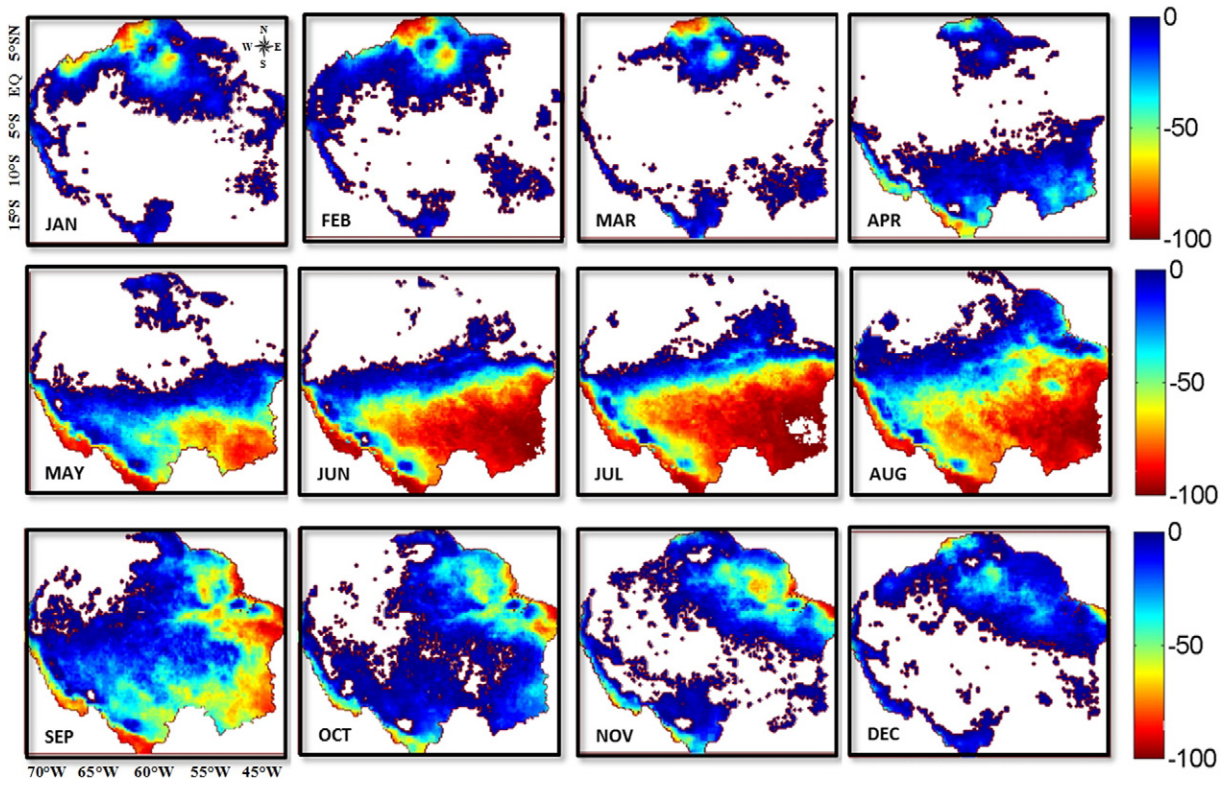

Fig. 4. Monthly estimates of water deficit (in mm month^{-1}), based on TRMM observations from 1998 to 2012. Areas with low water deficit are shown in blue, whereas the red color indicates high water deficits; areas with no water deficit are presented without color.

been published. Their usefulness to derive MODIS anisotropy will have to be addressed separately.

The ability of multi-angle observation to derive vegetation structural attributes is well supported by previous studies of temperate ecosystems (Chen et al., 2003; Gao, 2003). Multi-angle data decrease the dispersion and saturation in geometrically complex canopies (Zhang, Tian, Myneni, Knyazikhin, & Woodcock, 2002) and are therefore better suited to describe the three dimensional structure of forests compared to mono-angle acquisitions (Chen & Leblanc, 1997; A.H. Strahler & D.L.B. Jupp, 1990). Our strong linear relationship found between anisotropy and LAI estimates (Fig. 3a and b, $r^2 = 0.70$, $r^2 = 0.88$ $p < 0.05$, respectively) confirms these findings.

The RMSE for the relationships between anisotropy and field observations has allowed us to link seasonal changes in anisotropy with changes in vegetation structure. However, we do acknowledge that other structural variables can influence seasonal patterns of anisotropy in different ways. For instance, anisotropy is also affected by canopy roughness (Strahler, 2009), leaf angle distribution (Roujean, 2002)

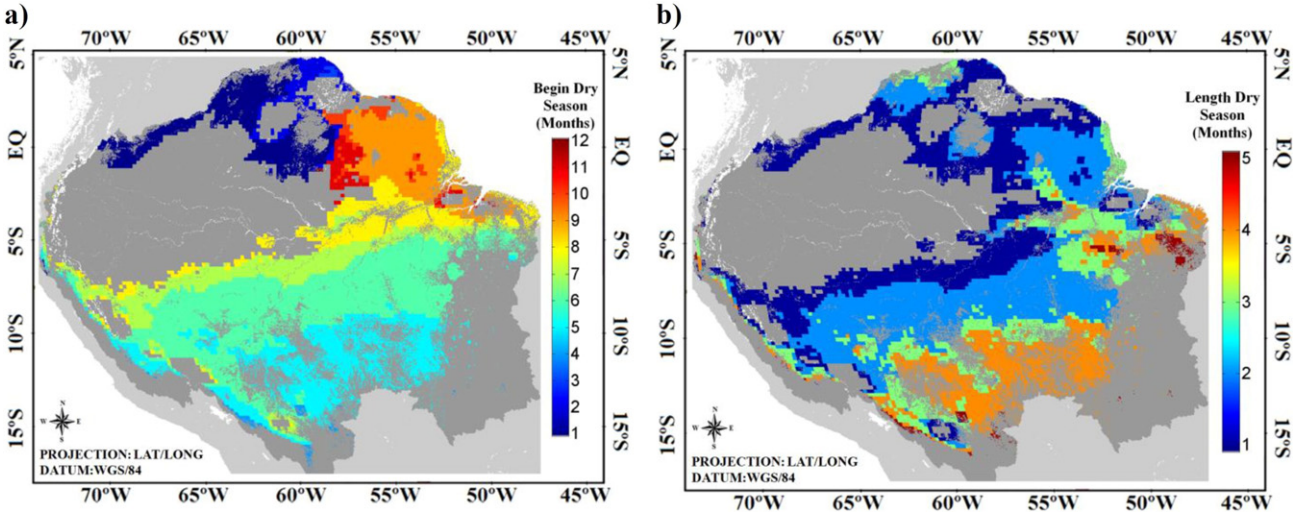

Fig. 5. Beginning (a) and length (b) of dry season across the Amazon calculated on per pixel basis using monthly water deficits. This approach was performed for each year separately in order to consider inter-annual variability. The figure shows mean onset and length of dry season for all years.

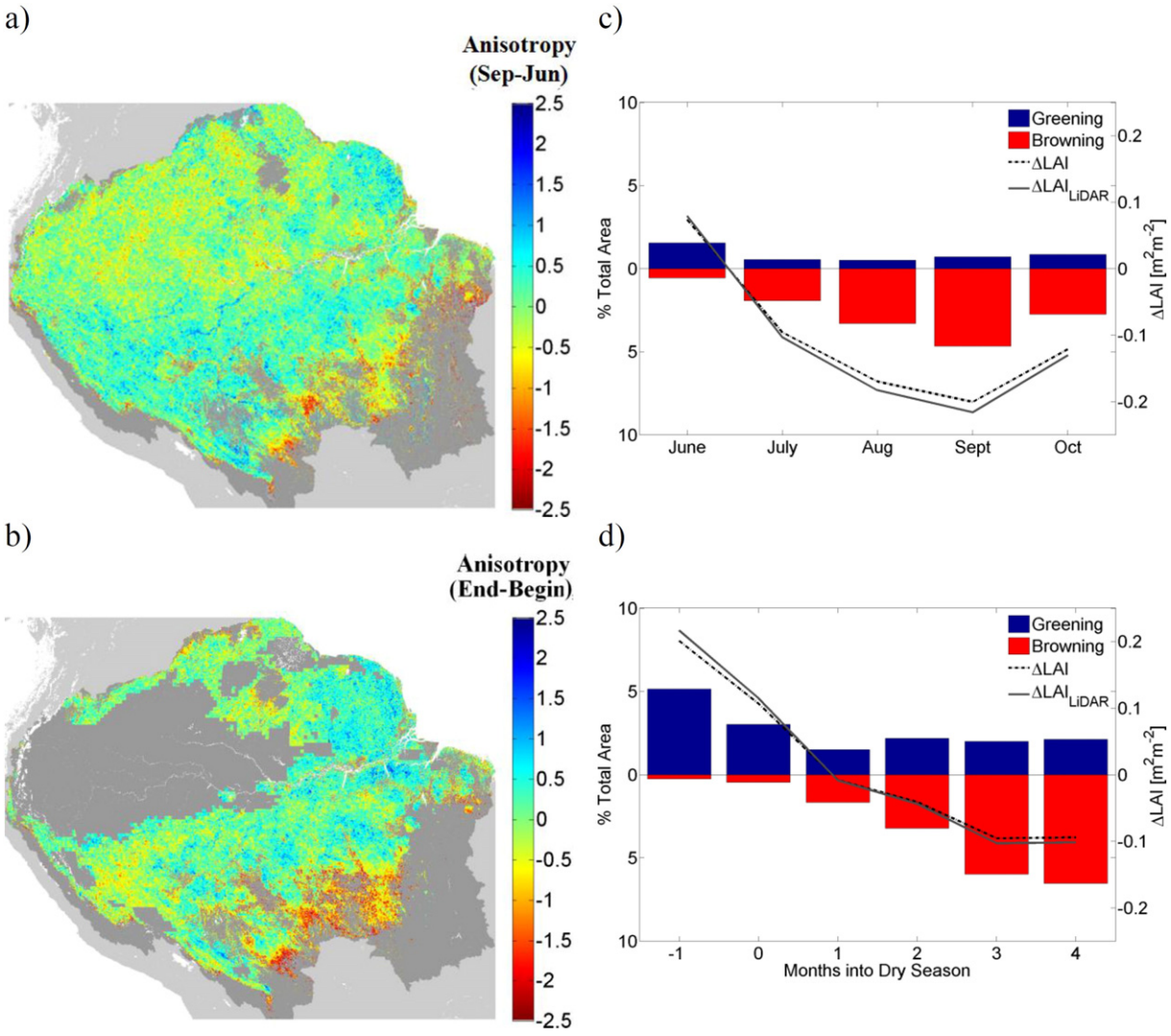

Fig. 6. (a) Spatial distribution of changes in anisotropy normalized by the standard deviation using a dry season period from June to September (for all years between 2000 and 2012, except 2005 and 2010). The gray regions represents no dry season or non-forested areas. (b) Spatial distribution of changes in anisotropy normalized by the standard deviation using specifc begin and end of dry season based on the water deficit maps. Figures c and d show the corresponding changes in greening (blue bars) and browning (red bars) by months of dry season ($p = 0.05$). The dashed lines in Figures c and d represent the net changes in LAI (averaged across the basin) modeled by the linear relationship between anisotropy and LAI (Fig. 2a). The solid line shows the corresponding estimates based on the model derived from LiDAR (Fig. 2b).

and foliage clumping (Chen et al., 2005). Furthermore, the selected approach of modeling LAI from LiDAR depends, to some extent, on footprint size and point density. While the technique utilized here has been validated elsewhere (Coops et al., 2007, Lovell et al., 2003), differences in ecosystem types and LiDAR configuration may affect LAI estimates. As a result, the findings presented with respect to changes in leaf area should be interpreted with care and should be understood more as an example of how anisotropy may be linked to structural variables. Further analysis will be required with respect to changes in anisotropy as a result of changes in canopy roughness or other parameters. Nonetheless, the linear functional form suggests that multi-angle observations may provide an opportunity to address current limitations caused by saturation of conventional (nadir) vegetation indices (Huete et al., 2006; Knyazikhin et al., 1998) at least within the range of observed LAI ($\leq 7\ m^2\ m^{-2}$).

While mono-angle observations have been shown to indicate levels of vegetation greenness, they are less well suited to describe the three dimensional structure of forest canopies (Chen & Leblanc, 1997; A.H. Strahler & D.L.B. Jupp, 1990). The selected approach using anisotropy may provide new insights into structural variability of Amazon forests as it increases the sensitivity of optical observations to changes across dense vegetation types. This should considerably improve our understanding of Amazon forest seasonality and drought tolerance.

The findings presented in Figs. 4 and 5 suggest that rainfall patterns in Amazonian forests varied greatly, causing differences in seasonality across the region. Estimates of water deficit (Fig. 5a and b), followed a south-west north-east gradient with up to 5 months of water deficit in the south-west whereas large areas of Amazonas state showed, on average, no water deficit during the observed years (compare Steege & Pitman, 2003). Previous research has suggested that vegetation seasonality may follow this gradient closely, as higher precipitation levels support higher leaf areas in the wetter regions while vegetation in drier areas is limited by available soil water (Myneni et al., 2007). Water availability may further contribute to changes in the spatial distribution of leaves (Guan et al., 2015; Malhado & Costa, 2009; Schurr et al., 2012; ter Steege et al., 2006; Wagner et al., 2013). Also, the length of dry season has been shown to correlate with above ground biomass (Saatchi, Houghton, Dos Santos Alvala, Soares, & Yu, 2007) and tree

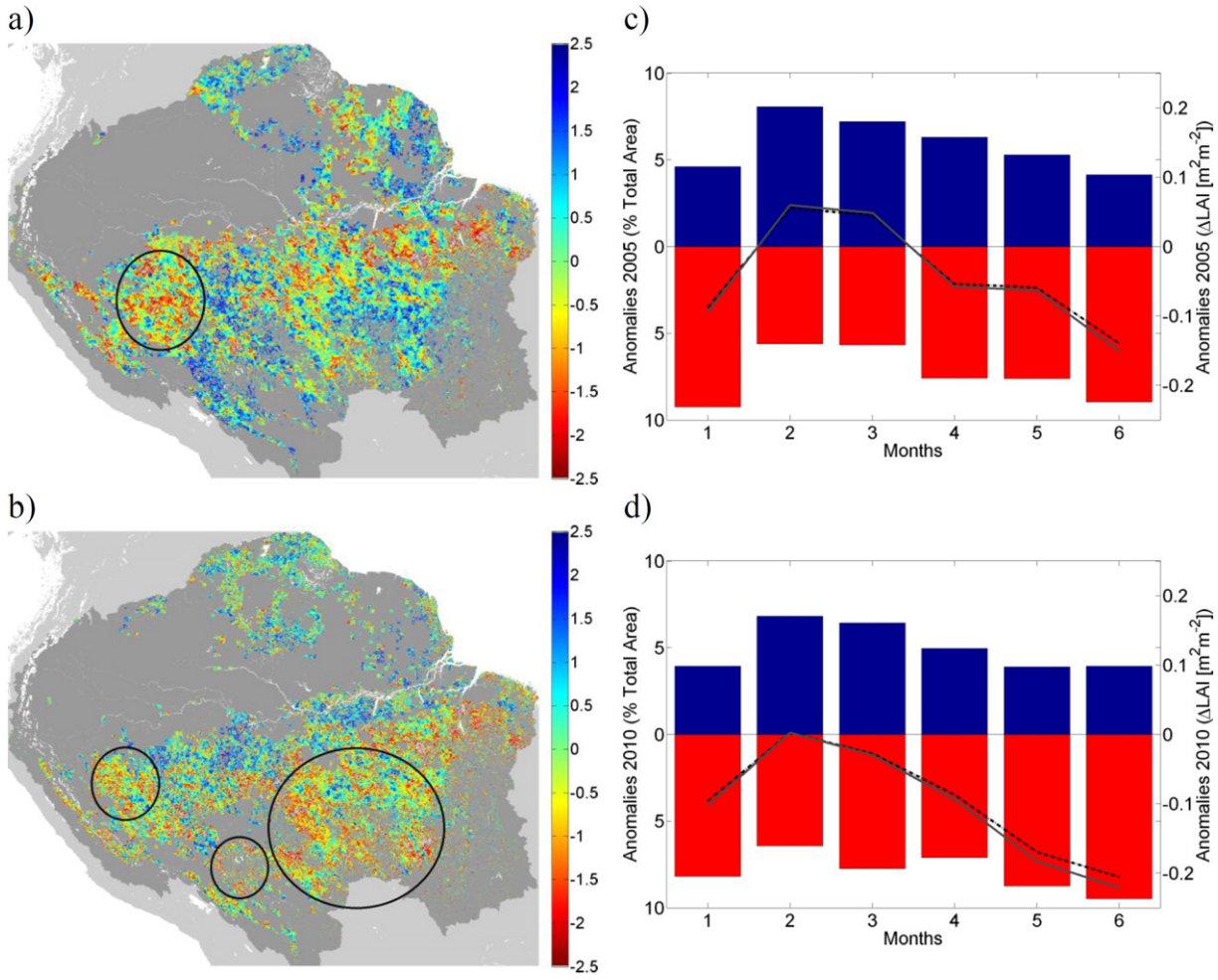

Fig. 7. Spatial distribution of the standardized anomalies in anisotropy for 2005 (a) and 2010 (b), considering specifically begin and end of dry season (based on the water deficit maps). The gray regions represents no dry season or non-forested areas. Figures c and d show the corresponding anomalies in greening (blue bars) and browning (red bars) by months into dry season ($p = 0.05$). Circles represents an approximation of the epicenters of the droughts described by Lewis et al. (2011). The dashed lines in Figures c and d represent the anomalies in LAI (averaged across the basin) modeled by the linear relationship between anisotropy and LAI (Fig. 2a). The solid line shows the corresponding estimates based on the model derived from LiDAR (Fig. 2b).

species composition (ter Steege et al., 2006; Wagner et al., 2014). Estimating vegetation seasonality from water deficit provided a simple but effective approach to capture this regional variability in precipitation. Other approaches, for example, based on available photosynthetically active radiation (PAR) are possible and may result in different definition of dry and wet season.

While our findings are in good agreement with previous reports (Steege & Pitman, 2003), it should be noted that in the northern part of the Amazon, cloud cover is considerably higher than in the south, which may increase measurement noise in the TRMM data and contribute to larger spatial variation in onset and length of dry season observed. The findings provided in Figs. 2, A.1 and 6 suggest large spatial and seasonal variability of Amazonian forests. This result relates well to previous studies on vegetation structure and seasonality of the Amazon (ter Steege et al., 2006; Villar et al., 2009) as well as estimates of aboveground carbon (Saatchi et al., 2011). Consideration of this variability will be critical for interpreting the biophysical responses of vegetation to changes in climate.

The results presented in Figs. 6 and 7 confirm seasonal swings in the Amazon (Myneni et al., 2007). While the total area with significant change (Fig. 6) is relatively small compared to Myneni et al. (2007), these variations can be explained by the difference in methods applied. First, Myneni et al. (2007) used the RMSE of the relationship to field observations to determine whether a change is significant or not, but did not normalize by the standard deviation. Our results in Fig. A.1 showed much increase seasonality when using the RMSE of field and LiDAR data (Fig. 3a and b) to determine significance. Also, Myneni et al. (2007) calculated seasonality as the difference between the maximum 4-month average LAI in the dry season minus the minimum 4-month average LAI in the wet season for those regions with dry seasons longer than 3 months. For all other regions, they calculated seasonality as the difference between the dry-season average LAI and the minimum 4-month average LAI in the wet season.

The seasonality in anisotropy (Figs. 1, 6) cannot be explained by directional effects, as all observations have been normalized to a fixed forward and backscatter geometry (Lyapustin, Wang, Laszlo, & Hilker, 2012). Opposite findings based on conventional MODIS data (Morton et al., 2014) will require further analysis to be addressed separately. One possible explanation might be noise in the dataset (Hilker et al., 2012) rendering residual changes below a statistical significance level. Changes in anisotropy (greening/browning) during the dry season (Figs. A.1, 6 and 7) coincided well with previous reports on Amazon seasonality. The results support the view that photosynthetic activity initially increases during the dry season in response to an increase in incident PAR (Brando et al., 2010; Graham et al., 2003; Huete et al., 2006; Hutyra et al., 2007; Malhi, Aragão, Galbraith, et al., 2009, Malhi,

Aragão, Metcalfe, et al., 2009; Myneni et al., 2007; Samanta et al., 2012; Wagner et al., 2013) while water supply is maintained through deep root systems of tropical forests (Nepstad et al., 1994).

Consistent to these findings, Fig. 6c and d showed an initial increase and then a decline in anisotropy after extended drought periods. While the fixed dry season assumption resulted in less clear trends, particularly with respect to area greening, the spatially explicit estimates of dry season onset and dry season length showed clear greening during the dry season onset. On the other hand, after an extended length of the dry season, this effect turned into net browning across areas that experienced 3 or more months of dry season in a given year.

The spatial and temporal patterns of anomalies in anisotropy for the 2005 and 2010 droughts (Fig. 7) allow the conclusions that although productivity of tropical vegetation may increase initially during the dry season (Brando et al., 2010; Graham et al., 2003; Huete et al., 2006), sustained drought reduces photosynthesis, canopy leaf area and ultimately causes tree mortality (Brando et al., 2008; Doughty et al., 2015; Phillips et al., 2009; Saleska et al., 2007). This is an important result as it helps reconcile findings from field and modeling studies with remote sensing observations — a key requirement for improving our understanding of drought behavior and quantifying carbon dynamics across vegetation and moisture gradients in Amazonia (Baker et al., 2008).

During both drought events (Fig. 7c and d), positive and negative anomalies were roughly balanced at the beginning of the dry season, indicating an expected natural variability in one year compared to the mean of all other years. However, browning effects became increasingly prominent, especially during 2010, where the size of areas with negative anomalies was almost three times larger than areas with greening. These strong anomalies may be explained by more intense water deficits causing faster depletion of available water supply and an extended duration of the dry season resulting in prolonged stress events. The spatial patterns presented for the two extensive droughts in the Amazon region were roughly in agreement with the regions of high drought intensity described in Lewis et al., 2011, with a concentration in the southwest for 2005, and more widespread effects in 2010 throughout the southeast. Our findings relate well also to plot and LiDAR-based studies, which showed that forest structure and density can be strongly affected by extreme droughts with significant reduction of forest productivity and above ground biomass over time (Phillips et al., 2009; Saatchi et al., 2013).

5. Conclusions

The findings presented in this study contribute to the recent debate on Amazon seasonality and drought tolerance in three major ways. First, we have demonstrated, using reflectance anisotropy obtained from multi-angle MODIS observations that Amazonian forests expose a large heterogeneity both spatially and seasonally and that this heterogeneity is related to differences in vegetation structure. The demonstrated approach using anisotropy may allow us to better detect and quantify these changes even in densely vegetated areas typical for tropical ecosystems. Second, our analysis has shown that quantification of seasonal changes in vegetation depends on the definition of onset and duration of the dry season. This conclusion underlines the need for explicit consideration of temporal differences, as the assumption of a fixed period of dry season may lead to erroneous conclusions about phenological cycles in Amazonian forests. Finally, our analysis reconciles remote sensing studies with field based observations and model results as it provides a sounder basis for the argument that tropical vegetation undergoes strong seasonal effects, leading to increased growth during the beginning of the dry season, but to vegetation decline after extended drought periods, particularly during the 2005 and 2010 extreme events.

Acknowledgment

We are grateful to the NASA Center for Climate Simulation (NCCS) for computational support and access to their high performance cluster. MAIAC data for the Amazon Basin was obtained from NASA's Level 1 Atmosphere Archive and Distribution System (LAADS Web) ftp://ladsweb.nascom.nasa.gov/MAIAC. We would like to thank Dr. Michael Keller for the helpful comments. LiDAR data for this study were obtained from the "Sustainable Landscapes Brazil" project, operated as a cooperation between EMBRAPA and the U.S. Forest Service (http://mapas.cnpm.embrapa.br/paisagenssustentaveis/). This study was partially funded by CAPES (Coordenação de Aperfeiçoamento de Pessoal de Nível Superior), grant number 12881-13-9; and CNPq (Conselho Nacional de Desenvolvimento Científico e Tecnológico), grant number PVE 401025/2014-4. L.O.A thanks UK NERC *Amazonica* grant NE/F005482/1 and FAPESP grant 2013/50533-5.

Appendix A

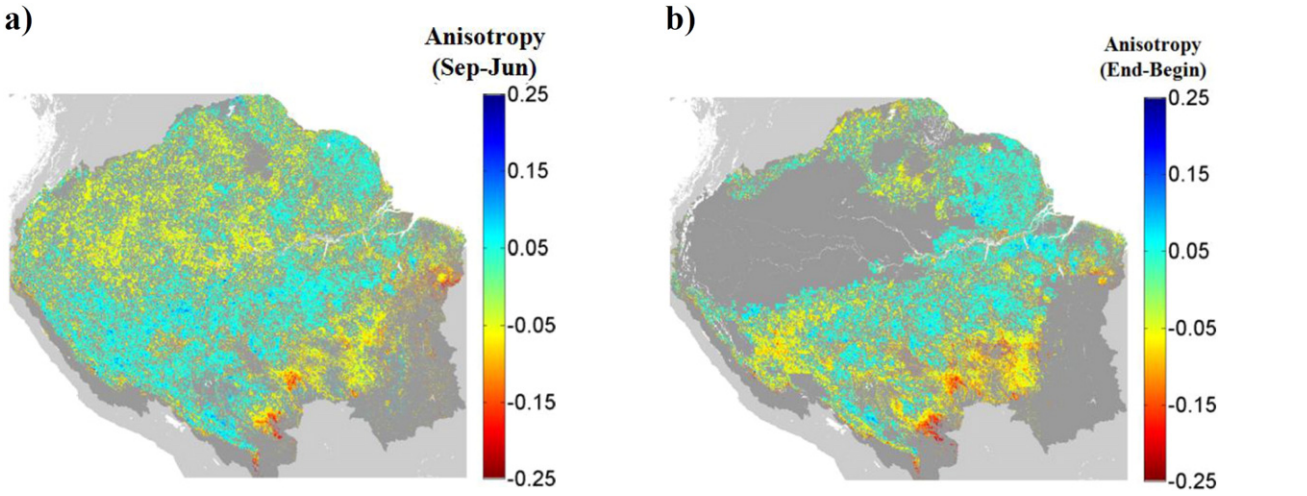

Fig. A.1. (a) Spatial distribution of changes in non-normalized anisotropy normalized using a dry season period from June to October (for all years, except 2005 and 2010). The gray regions represents no dry season or non-forested areas. (b) Spatial distribution of changes in non-normalized anisotropy using specifc begin and end of dry season based on the water deficit maps.

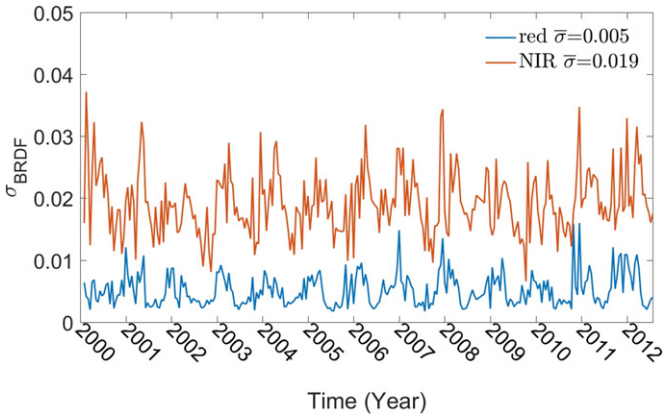

Fig. A.2. Temporal variability of the standard deviation between observed and modeled MAIAC reflectance (red and NIR). The graph represents an area of 100 × 100 km to obtain sufficient statistics given high cloud cover in the Amazon (65°0′0″ W, 5°0′0″ S).

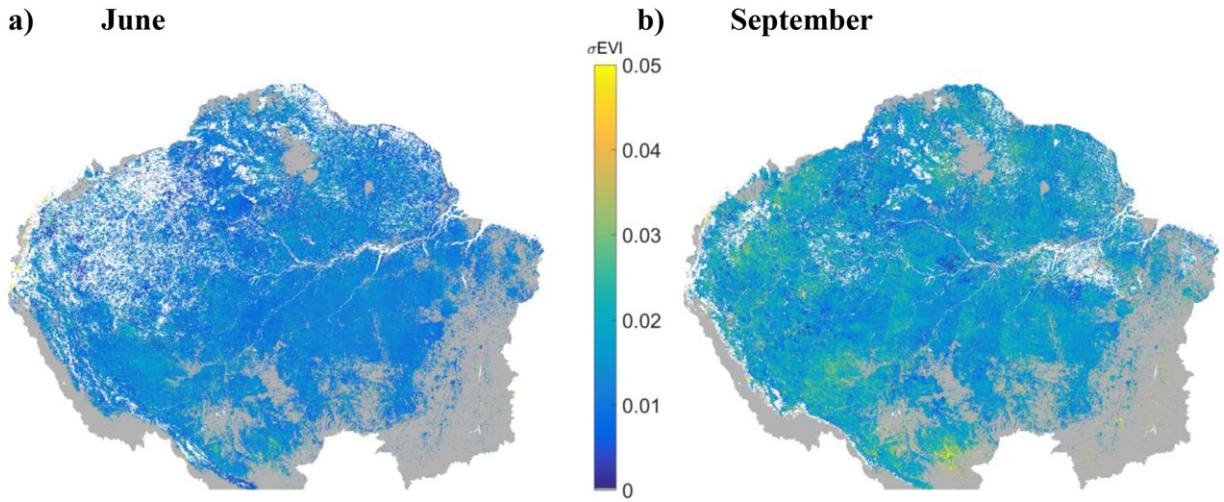

Fig. A.3. Spatial variability of the standard deviation between observed and modeled MAIAC EVI (a) in June and (b) in September. Data were averaged over a 30 day period to obtain sufficient statistics given high cloud cover in the Amazon.

References

Anderson, L. O. (2012). Biome-scale forest properties in Amazonia based on field and satellite observations. *Remote Sensing*, *4*(12), 1245–1271. http://dx.doi.org/10.3390/rs4051245.

Andreae, M. O. (2002). Biogeochemical cycling of carbon, water, energy, trace gases, and aerosols in Amazonia: The LBA-EUSTACH experiments. *Journal of Geophysical Research*, *107*(D20), 8066. http://dx.doi.org/10.1029/2001JD000524.

Aragao, L. E. O. C., Liana, O., Malhi, Y., Roman-Cuesta, R. M., Saatchi, S., & Edemir, Y. (2007). Spatial patterns and fire response of recent Amazonian droughts. *Geophysical Research Letters*, *34*, 1–5 (Retrieved from http://www.yadvindermalhi.org/uploads/1/8/7/6/18767612/aragao-2007-spatial_patterns_and_fire_response_of_recent_amazonian_droughts.pdf).

Asner, G. P., & Alencar, A. (2010). Drought impacts on the Amazon forest: The remote sensing perspective. *The New Phytologist*, *187*(3), 569–578. http://dx.doi.org/10.1111/j.1469-8137.2010.03310.x.

Asner, G. P., Nepstad, D., Cardinot, G., & Ray, D. (2004). Drought stress and carbon uptake in an Amazon forest measured with spaceborne imaging spectroscopy. *Proceedings of the National Academy of Sciences of the United States of America*http://dx.doi.org/10.1073/pnas.0400168101.

Atkinson, P. M., Dash, J., & Jeganathan, C. (2011). Amazon vegetation greenness as measured by satellite sensors over the last decade. *Geophysical Research Letters*, *38*(19) http://dx.doi.org/10.1029/2011GL049118 (n/a–n/a).

Baker, I. T., Prihodko, L., Denning, A. S., Goulden, M., Miller, S., & da Rocha, H. R. (2008). Seasonal drought stress in the Amazon: Reconciling models and observations. *Journal of Geophysical Research*, *113*, G00B01. http://dx.doi.org/10.1029/2007JG000644.

Barnsley, M. J., Settle, J. J., Cutter, M. A., Lobb, D. R., & Teston, F. (2004). The PROBA/CHRIS mission: A low-cost smallsat for hyperspectral multiangle observations of the Earth surface and atmosphere. *IEEE Transactions on Geoscience and Remote Sensing*, *42*(7), 1512–1520. http://dx.doi.org/10.1109/TGRS.2004.827260.

Bicheron, P. (1999). A method of biophysical parameter retrieval at global scale by inversion of a vegetation reflectance model. *Remote Sensing of Environment*, *67*(3), 251–266. http://dx.doi.org/10.1016/S0034-4257(98)00083-2.

Borchert, R. (1998). Responses of tropical trees to rainfall seasonality and its long-term changes. *Potential Impacts of Climate Change on Tropical Forest Ecosystems*. (pp. 241–253) Netherlands: Springer.

Brando, P. M., Goetz, S. J., Baccini, A., Nepstad, D. C., Beck, P. S. A., & Christman, M. C. (2010). Seasonal and interannual variability of climate and vegetation indices across the Amazon. *Proceedings of the National Academy of Sciences of the United States of America*, *107*(33), 14685–14690. http://dx.doi.org/10.1073/pnas.0908741107.

Brando, P. M., Nepstad, D. C., Davidson, E. A., Trumbore, S. E., Ray, D., & Camargo, P. (2008). Drought effects on litterfall, wood production and belowground carbon cycling in an Amazon forest: Results of a throughfall reduction experiment. *Philosophical Transactions of the Royal Society of London. Series B, Biological Sciences*, *363*(1498), 1839–1848. http://dx.doi.org/10.1098/rstb.2007.0031.

Carlson, T. N., & Ripley, D. A. (1997). On the relation between NDVI, fractional vegetation cover, and leaf area index. *Remote Sensing of Environment*, *62*(3), 241–252. http://dx.doi.org/10.1016/S0034-4257(97)00104-1.

Chen, J. M., & Leblanc, S. G. (1997). A four-scale bidirectional reflectance model based on canopy architecture. *IEEE Transactions on Geoscience and Remote Sensing*, *35*(5), 1316–1337. http://dx.doi.org/10.1109/36.628798.

Chen, J. M., Liu, J., Leblanc, S. G., Lacaze, R., & Roujean, J. -L. (2003). Multi-angular optical remote sensing for assessing vegetation structure and carbon absorption. *Remote Sensing of Environment*, *84*(4), 516–525. http://dx.doi.org/10.1016/S0034-4257(02)00150-5.

Chen, J. M., Menges, C. H., & Leblanc, S. G. (2005). Global mapping of foliage clumping index using multi-angular satellite data. *Remote Sensing of Environment*, *97*(4), 447–457. http://dx.doi.org/10.1016/j.rse.2005.05.003.

Coops, N. C., Hilker, T., Wulder, M. A., St-Onge, B., Newnham, G., Siggins, A., & Trofymow, J. A. (2007). Estimating canopy structure of Douglas-fir forest stands from discrete-return LiDAR. *Trees*, *21*(3), 295–310. http://dx.doi.org/10.1007/s00468-006-0119-6.

Diner, D. J., Beckert, J. C., Reilly, T. H., Bruegge, C. J., Conel, J. E., Kahn, R. A., ... Verstraete, M. M. (1998r). Multi-angle Imaging SpectroRadiometer (MISR) instrument description

and experiment overview. *IEEE Transactions on Geoscience and Remote Sensing*, *36*(4), 1072–1087. http://dx.doi.org/10.1109/36.700992.

Domingues, T. F., Berry, J. A., Martinelli, L. A., Ometto, J. P. H. B., & Ehleringer, J. R. (2005). Parameterization of canopy structure and leaf-level gas exchange for an eastern amazonian tropical rain forest (tapajós national forest, Pará, Brazil). *Earth Interactions*, *9*(17), 1–23. http://dx.doi.org/10.1175/EI149.1.

Doughty, C. E., & Goulden, M. L. (2008a). Are tropical forests near a high temperature threshold? *Journal of Geophysical Research*, *113*, G00B07. http://dx.doi.org/10.1029/2007JG000632.

Doughty, C. E., & Goulden, M. L. (2008b). Seasonal patterns of tropical forest leaf area index and CO_2 exchange. *Journal of Geophysical Research*, *113*, G00B06. http://dx.doi.org/10.1029/2007JG000590.

Doughty, C. E., & Goulden, M. L. (2008c). Are tropical forests near a high temperature threshold? *Journal of Geophysical Research: Biogeosciences*, *113*(2005–2012) (G1).

Doughty, C. E., Metcalfe, D. B., Girardin, C. A. J., Amézquita, F. F., Cabrera, D. G., Huasco, W. H., ... Malhi, Y. (2015-). Drought impact on forest carbon dynamics and fluxes in Amazonia. *Nature*, *519*(7541), 78–82. http://dx.doi.org/10.1038/nature14213.

Figuera, A. M. S., de Sousa, C. A. D., Menton, M. C., Juarez, R. N., da Rocha, H. R., Miller, S. D., & Goulden, M. L. (2011,). *). LBA-ECO CD-04 leaf area index, km 83 tower site, Tapajos National Forest, Brazil. Data Set. Available on-Line [http://daac.ornl.gov] from.* Oak Ridge, Tennessee, U.S.A.: Oak Ridge National Laboratory Distributed Active Archive Center. http://dx.doi.org/10.3334/ORNLDAAC/992.

Franch, B., Vermote, E. F., Sobrino, J. a., & Fédèle, E. (2013). Analysis of directional effects on atmospheric correction. *Remote Sensing of Environment*, *128*, 276–288. http://dx.doi.org/10.1016/j.rse.2012.10.018.

Friedl, M. A., Sulla-Menashe, D., Tan, B., Schneider, A., Ramankutty, N., Sibley, A., & Huang, X. (2010a). MODIS Collection 5 global land cover: Algorithm refinements and characterization of new datasets. *Remote Sensing of Environment*, *114*(1), 168–182. http://dx.doi.org/10.1016/j.rse.2009.08.016.

Fu, R., Yin, L., Li, W., Arias, P. A., Dickinson, R. E., Huang, L., & Chakraborty, S. (2013). Increased dry-season length over southern Amazonia in recent decades and its implication for future climate projection. *Proceedings of the National Academy of Sciences of the United States of America*, *110*(45)http://dx.doi.org/10.1073/pnas.1302584110.

Galvao, L. S., dos Santos, J. R., Roberts, D. a., Breunig, F., Marcelo, B., Toomey, M., & de Moura, Y. M. (2011r). On intra-annual EVI variability in the dry season of tropical forest: A case study with MODIS and hyperspectral data. *Remote Sensing of Environment*, *115*(9), 2350–2359. http://dx.doi.org/10.1016/j.rse.2011.04.035.

Gao, F. (2003). Detecting vegetation structure using a kernel-based BRDF model. *Remote Sensing of Environment*, *86*(2), 198–205. http://dx.doi.org/10.1016/S0034-4257(03)00100-7.

Gatti, L. V., Gloor, M., Miller, J. B., Doughty, C. E., Malhi, Y., Domingues, L. G., ... Lloyd, J. (2014e). Drought sensitivity of Amazonian carbon balance revealed by atmospheric measurements. *Nature*, *506*(7486), 76–80. http://dx.doi.org/10.1038/nature12957.

Graham, E. A., Mulkey, S. S., Kitajima, K., Phillips, N. G., & Wright, S. J. (2003). Cloud cover limits net CO_2 uptake and growth of a rainforest tree during tropical rainy seasons. *Proceedings of the National Academy of Sciences of the United States of America*, *100*(2), 572–576. http://dx.doi.org/10.1073/pnas.0133045100.

Guan, K., Pan, M., Li, H., Wolf, A., Wu, J., Medvigy, D., ... Lyapustin, A. I. (2015h). Photosynthetic seasonality of global tropical forests constrained by hydroclimate. *Nature Geoscience*. http://dx.doi.org/10.1038/ngeo2382.

Hilker, T., Lyapustin, A. I., Hall, F. G., Myneni, R., Knyazikhin, Y., Wang, Y., ... Sellers, P. J. (2015l). On the measurability of change in Amazon vegetation from MODIS. *Remote Sensing of Environment*, *166*, 233–242. http://dx.doi.org/10.1016/j.rse.2015.05.020.

Hilker, T., Lyapustin, A. I., Tucker, C. J., Hall, F. G., Myneni, R. B., Wang, Y., ... Sellers, P. J. (2014o). Vegetation dynamics and rainfall sensitivity of the Amazon. *Proceedings of the National Academy of Sciences*, *111*(45), 16041–16046. http://dx.doi.org/10.1073/pnas.1404870111.

Hilker, T., Lyapustin, A. I., Tucker, C. J., Sellers, P. J., Hall, F. G., & Wang, Y. (2012). Remote sensing of tropical ecosystems: Atmospheric correction and cloud masking matter. *Remote Sensing of Environment*, *127*, 370–384. http://dx.doi.org/10.1016/j.rse.2012.08.035.

Hilker, T., Wulder, M. A., Coops, N. C., Linke, J., McDermid, G., Masek, J. G., ... White, J. C. (2009). A new data fusion model for high spatial- and temporal-resolution mapping of forest disturbance based on Landsat and MODIS. *Remote Sensing of Environment*, *113*(8), 1613–1627. http://dx.doi.org/10.1016/j.rse.2009.03.007.

Huete, A. R., Didan, K., Shimabukuro, Y. E., Ratana, P., Saleska, S. R., Hutyra, L. R., ... Myneni, R. (2006n). Amazon rainforests green-up with sunlight in dry season. *Geophysical Research Letters*, *33*(6), L06405. http://dx.doi.org/10.1029/2005GL025583.

Huete, A., Didan, K., Miura, T., Rodriguez, E. P., Gao, X., & Ferreira, L. G. (2002). Overview of the radiometric and biophysical performance of the MODIS vegetation indices. *Remote Sensing of Environment*, *83*(1–2), 195–213.

Hutyra, L. R., Munger, J. W., Saleska, S. R., Gottlieb, E., Daube, B. C., Dunn, A. L., ... Wofsy, S. C. (2007a). Seasonal controls on the exchange of carbon and water in an Amazonian rain forest. *Journal of Geophysical Research*, *112*(G3), G03008. http://dx.doi.org/10.1029/2006JG000365.

Knyazikhin, Y., Martonchik, J. V., Diner, D. J., Myneni, R. B., Verstraete, M., Pinty, B., & Gobron, N. (1998r). Estimation of vegetation canopy leaf area index and fraction of absorbed photosynthetically active radiation from atmosphere-corrected MISR data. *Journal of Geophysical Research*, *103*(D24), 32239. http://dx.doi.org/10.1029/98JD02461.

Leblanc, S. G., Chen, J. M., White, H. P., Latifovic, R., Lacaze, R., & Roujean, J. -L. (2005). Canada-wide foliage clumping index mapping from multiangular POLDER measurements. *Canadian Journal of Remote Sensing*, *31*(5), 364–376. http://dx.doi.org/10.5589/m05-020.

Lewis, S. L., Brando, P. M., Phillips, O. L., van der Heijden, G. M. F., & Nepstad, D. (2011). The 2010 Amazon drought. *Science (New York, N.Y.)*, *331*(6017), 554.

Lovell, J. L., Jupp, D. L. B., Culvenor, D. S., & Coops, N. C. (2003). Using airborne and ground-based ranging lidar to measure canopy structure in Australian forests. *Canadian Journal of Remote Sensing*, *29*(5), 607–622. http://dx.doi.org/10.5589/m03-026.

Lyapustin, A., & Knyazikhin, Y. (2001). *Green' s function method for the radiative transfer40. (pp. 3495–3501), 3495–3501.*

Lyapustin, A. I., & Muldashev, T. Z. (1999). Method of spherical harmonics in the radiative transfer problem with non-Lambertian surface. *Journal of Quantitative Spectroscopy and Radiative Transfer*, *61*(4), 545–555. http://dx.doi.org/10.1016/S0022-4073(98)00041-7.

Lyapustin, A. I., Wang, Y., Laszlo, I., Hilker, T., Hall, F. G., Sellers, P. J., ... Korkin, S. V. (2012n). Multi-angle implementation of atmospheric correction for MODIS (MAIAC): 3. Atmospheric correction. *Remote Sensing of Environment*, *127*, 385–393. http://dx.doi.org/10.1016/j.rse.2012.09.002.

Lyapustin, A., Martonchik, J., Wang, Y., Laszlo, I., & Korkin, S. (2011). Multiangle implementation of atmospheric correction (MAIAC): 1. Radiative transfer basis and look-up tables. *Journal of Geophysical Research*, *116*(D3), D03210. http://dx.doi.org/10.1029/2010JD014985.

Lyapustin, A., Wang, Y., Laszlo, I., & Hilker, T. (2012b). Multi-angle implementation of atmospheric correction for MODIS (MAIAC). Part 3: Atmospheric correction. *Remote Sensing of Environment*, *127*, 385–393.

Lyapustin, A., Wang, Y., Xiong, X., Meister, G., Platnick, S., Levy, R., ... Angal, A. (2014,). Science impact of MODIS C5 calibration degradation and C6+ improvements. *Atmospheric Measurement Techniques Discussions*, *7*(7), 7281–7319. http://dx.doi.org/10.5194/amtd-7-7281-2014.

Malhado, A., & Costa, M. (2009). Seasonal leaf dynamics in an Amazonian tropical forest. *Forest ecology and management*, *258*(7), 1161–1165.

Malhi, Y., Aragão, L. E. O. C., Galbraith, D., Huntingford, C., Fisher, R., Zelazowski, P., ... Meir, P. (2009c). Exploring the likelihood and mechanism of a climate-change-induced dieback of the Amazon rainforest. *Proceedings of the National Academy of Sciences of the United States of America*, *106*(49), 20610–20615. http://dx.doi.org/10.1073/pnas.0804619106.

Malhi, Y., Aragão, L. E. O. C., Metcalfe, D. B., Paiva, R., Quesada, C. A., Almeida, S., ... Teixeira, L. M. (2009a). Comprehensive assessment of carbon productivity, allocation and storage in three Amazonian forests. *Global Change Biology*, *15*(5), 1255–1274. http://dx.doi.org/10.1111/j.1365-2486.2008.01780.x.

Malhi, Y., Roberts, J. T., Betts, R. A., Killeen, T. J., Li, W., & Nobre, C. A. (2008). January 11 Climate change, deforestation, and the fate of the Amazon. *Science (New York, N.Y.)*http://dx.doi.org/10.1126/science.1146961.

Marengo, J. A., Nobre, C. A., Tomasella, J., Oyama, M. D., Sampaio de Oliveira, G., de Oliveira, R., ... Brown, I. F. (2008e). The drought of amazonia in 2005. *Journal of Climate*, *21*(3), 495–516. http://dx.doi.org/10.1175/2007JCLI1600.1.

Marengo, J. A., Tomasella, J., Alves, L. M., Soares, W. R., & Rodriguez, D. A. (2011). The drought of 2010 in the context of historical droughts in the Amazon region. *Geophysical Research Letters*, *38*(12). http://dx.doi.org/10.1029/2011GL047436.

Meir, P., Metcalfe, D. B., Costa, A. C. L., & Fisher, R. A. (2008). The fate of assimilated carbon during drought: impacts on respiration in Amazon rainforests. *Philosophical Transactions of the Royal Society of London. Series B, Biological Sciences*, *363*(1498), 1849–1855. http://dx.doi.org/10.1098/rstb.2007.0021.

Morton, D. C., Nagol, J., Carabajal, C. C., Rosette, J., Palace, M., Cook, B. D., ... North, P. R. J. (2014i). Amazon forests maintain consistent canopy structure and greenness during the dry season. *Nature*, 221–224. http://dx.doi.org/10.1038/nature13006 (*doi:10.103*(7487)).

Moura, Y. M., Galvão, L. S., dos Santos, J. R., Roberts, D. A., & Breunig, F. M. (2012). Use of MISR/Terra data to study intra- and inter-annual EVI variations in the dry season of tropical forest. *Remote Sensing of Environment*, *127*, 260–270. http://dx.doi.org/10.1016/j.rse.2012.09.013.

Myneni, R. B., Yang, W., Nemani, R. R., Huete, A. R., Dickinson, R. E., Knyazikhin, Y., ... Salomonson, V. V. (2007,). Large seasonal swings in leaf area of Amazon rainforests. *Proceedings of the National Academy of Sciences of the United States of America*, *104*(12), 4820–4823. http://dx.doi.org/10.1073/pnas.0611338104.

Myneni, R., Hoffman, S., Knyazikhin, Y., Privette, J., Glassy, J., Tian, Y., ... Running, S. (2002g). Global products of vegetation leaf area and fraction absorbed PAR from year one of MODIS data. *Remote Sensing of Environment*, *83*(1–2), 214–231. http://dx.doi.org/10.1016/S0034-4257(02)00074-3.

Negrón Juárez, R. I., da Rocha, H. R., eFigueira, A. M. S., Goulden, M. L., & Miller, S. D. (2009). An improved estimate of leaf area index based on the histogram analysis of hemispherical photographs. *Agricultural and Forest Meteorology*, *149*(6–7), 920–928. http://dx.doi.org/10.1016/j.agrformet.2008.11.012.

Nepstad, D. C., de Carvalho, C. R., Davidson, E. A., Jipp, P. H., Lefebvre, P. A., Negreiros, G. H., ... Vieira, S. (1994S). The role of deep roots in the hydrological and carbon cycles of Amazonian forests and pastures. *Nature*, *372*(6507), 666–669. http://dx.doi.org/10.1038/372666a0.

Phillips, O. L., Aragão, L. E. O. C., Lewis, S. L., Fisher, J. B., Lloyd, J., López-gonzález, G., Malhi, Y. , Monteagudo, A., Peacock, J., Quesada, C. A., Heijden, G., Der, V., Almeida, S., Amaral, I., Arroyo, L., Aymard, G., Baker, T. R., Bánki, O., ... Salamão, R. (2009,). *Drought sensitivity of the Amazon rainforest.* (Retrieved August 5, 2014, from http://www.sciencemag.org/content/323/5919/1344.full.pdf).

Reading, R. P., Bedunah, D. J., & Amgalanbaatar, S. (2006). Conserving biodiversity on Mongolian rangelands: implications for protected area development and pastoral uses. *Rangelands of Central Asia* Proceedings of the Cconference on Ttransformations, Iissues, and Ffuture Cchallenges, USDA Forest Service Proceedings RMRS-P-39 [Available at: http://www. fs. fed. us/rm/pubs/rmrs_p039/rmrs_p039_001_017. pdf].

Restrepo-Coupe, N., da Rocha, H. R., Hutyra, L. R., da Araujo, A. C., Borma, L. S., Christoffersen, B., Cabral, O. M. R., de Camargo, P. B., Cardoso, F. L., da Costa, A. C. L., Fitzjarrald, D. R., Goulden, M. L., Kruijt, B., Maia, J. M. F., Malhi, Y. S., Manzi, A. O., Miller, S. D., ... Saleska, S. R. (2013r). What drives the seasonality of photosynthesis

across the Amazon Basin? A cross-site analysis of eddy flux tower measurements from the Brasil flux network. *Agricultural and Forest Meteorology*, *182-183*, 128–144. http://dx.doi.org/10.1016/j.agrformet.2013.04.031.

Roujean, J. -L. (2002). Global mapping of vegetation parameters from POLDER multiangular measurements for studies of surface-atmosphere interactions: A pragmatic method and its validation. *Journal of Geophysical Research*, *107*(D12), 4150. http://dx.doi.org/10.1029/2001JD000751.

Roujean, J. -L., Leroy, M., & Deschamps, P. -Y. (1992). *97*(92).

Saatchi, S. S., Harris, N. L., Brown, S., Lefsky, M., Mitchard, E. T. A., Salas, W., ... Morel, A. (2011n). Benchmark map of forest carbon stocks in tropical regions across three continents. *Proceedings of the National Academy of Sciences of the United States of America*, *108*(24), 9899–9904. http://dx.doi.org/10.1073/pnas.1019576108.

Saatchi, S., Asefi-Najafabady, S., Malhi, Y., Aragão, L. E. O. C., Anderson, L. O., Myneni, R. B., & Nemani, R. (2013e). Persistent effects of a severe drought on Amazonian forest canopy. *Proceedings of the National Academy of Sciences of the United States of America*, *110*(2), 565–570. http://dx.doi.org/10.1073/pnas.1204651110.

Saatchi, S., Houghton, R. A., Dos Santos Alvala, R. C., Soares, J. V., & Yu, Y. (2007). Distribution of aboveground live biomass in the Amazon basin. *Global Change Biology*, *13*(4), 816–837. http://dx.doi.org/10.1111/j.1365-2486.2007.01323.x.

Saleska, S. R., Didan, K., Huete, A. R., & da Rocha, H. R. (2007). Amazon forests green-up during 2005 drought. *Science (New York, N.Y.)*, *318*(5850), 612. http://dx.doi.org/10.1126/science.1146663.

Samanta, A., Ganguly, S., Hashimoto, H., Devadiga, S., Vermote, E., Knyazikhin, Y., ... Myneni, R. B. (2010m). Amazon forests did not green-up during the 2005 drought. *Geophysical Research Letters*, *37*(5)http://dx.doi.org/10.1029/2009GL042154 (n/a–n/a).

Samanta, A., Knyazikhin, Y., Xu, L., Dickinson, R. E., Fu, R., Costa, M. H., ... Myneni, R. B. (2012i). Seasonal changes in leaf area of Amazon forests from leaf flushing and abscission. *Journal of Geophysical Research*, *117*(G1), G01015http://dx.doi.org/10.1029/2011JG001818.

Schaaf, C. B., Gao, F., Strahler, A. H., Lucht, W., Li, X., Tsang, T., Strugnell, N. C., Zhang, X., Jin, Y., Muller, J. P., Lewis, P., Barnsley, M., Hobson, P., Disney, M., Roberts, G., Dunderdale, M., Doll, C., ... Roy, D. (2002,). First operational BRDF, albedo nadir reflectance products from MODIS. *Remote Sensing of Environment*, *83*(1–2), 135–148.

Schurr, F. M., Pagel, J., Cabral, J. S., Groeneveld, J., Bykova, O., O'Hara, R. B., ... Zimmermann, N. E. (2012s). How to understand species' niches and range dynamics: A demographic research agenda for biogeography. *Journal of Biogeography*, *39*(12), 2146–2162. http://dx.doi.org/10.1111/j.1365-2699.2012.02737.x.

Scurlock, J. M. O., Asner, G. P., & Gower, S. T. (2001). *Global leaf area index from field measurements, 1932–2000*. http://dx.doi.org/10.3334/ORNLDAAC/584.

Silva, F. B., Shimabukuro, Y. E., Aragão, L. E. O. C., Anderson, L. O., Pereira, G., Cardozo, F., & Arai, E. (2013,). Large-scale heterogeneity of Amazonian phenology revealed from 26-year long AVHRR/NDVI time-series. *Environmental Research Letters*, *8*(2), 024011. http://dx.doi.org/10.1088/1748-9326/8/2/024011.

Steege, H. T., Pitman, N., Sabatier, D., Castellanos, H., Van Der Hout, P., Daly, D. C., & Morawetz, W. (2003). A spatial model of tree α-diversity and tree density for the Amazon. *Biodiversity & Conservation*, *12*(11), 2255–2277.

Strahler, A., & Jupp, D. (1990b). Modeling bidirectional reflectance of forests and woodlands using Boolean models and geometric optics. *Remote Sensing of Environment*, *34*(3), 153–166.

Strahler, A. H. (2009). Vegetation canopy reflectance modeling—recent developments and remote sensing perspectives∗. *Remote Sensing Reviews*, *15*(1–4), 179–194. http://dx.doi.org/10.1080/02757259709532337.

Strahler, A. H., & Jupp, D. L. B. (1990a). Modeling bidirectional reflectance of forests and woodlands using boolean models and geometric optics. *Remote Sensing of Environment*, *34*(3), 153–166. http://dx.doi.org/10.1016/0034-4257(90)90065-T.

Ter Steege, H., Pitman, N. C. A., Phillips, O. L., Chave, J., Sabatier, D., Duque, A., ... Vásquez, R. (2006P). Continental-scale patterns of canopy tree composition and function across Amazonia. *Nature*, *443*(7110), 444–447. http://dx.doi.org/10.1038/nature05134.

Villar, E. C. J., Ronchail, J., Guyot, L., Cochonneau, G., Naziano, F., Lavado, W., ... Vauchel, P. (2009a). Spatio-temporal rainfall variability in the Amazon Basin countries (Brazil, Peru, Bolivia, Colombia, and Ecuador). *International Journal of Climatology*, *1594*(December 2008), 1574–1594. http://dx.doi.org/10.1002/joc.

Wagner, F., Rossi, V., Aubry-Kientz, M., Bonal, D., Dalitz, H., Gliniars, R., ... Hérault, B. (2014r). Pan-tropical analysis of climate effects on seasonal tree growth. *PLoS ONE*, *9*(3), e92337. http://dx.doi.org/10.1371/journal.pone.0092337.

Wagner, F., Rossi, V., Stahl, C., Bonal, D., & Hérault, B. (2013). Asynchronism in leaf and wood production in tropical forests: A study combining satellite and ground-based measurements. *Biogeosciences*, *10*(11), 7307–7321. http://dx.doi.org/10.5194/bg-10-7307-2013.

Walthall, C. L. (1997). A study of reflectance anisotropy and canopy structure using a simple empirical model. *Remote Sensing of Environment*, *128*(May 1995), 118–128.

Wang, Y., Lyapustin, A. I., Privette, J. L., Cook, R. B., SanthanaVannan, S. K., Vermote, E. F., & Schaaf, C. L. (2010a). Assessment of biases in MODIS surface reflectance due to lambertian approximation. *Remote Sensing of Environment*, *114*(11), 2791–2801. http://dx.doi.org/10.1016/j.rse.2010.06.013.

Widlowski, J. -L., Pinty, B., Gobron, N., Verstraete, M. M., Diner, D. J., & Davis, A. B. (2004). Canopy structure parameters derived from multi-angular remote sensing data for terrestrial carbon studies. *Climatic Change*, *67*(2–3), 403–415. http://dx.doi.org/10.1007/s10584-004-3566-3.

Widlowski, J. -L., Pinty, B., Lavergne, T., Verstraete, M. M., & Gobron, N. (2005). Using 1-D models to interpret the reflectance anisotropy of 3-D canopy targets: issues and caveats. *IEEE Transactions on Geoscience and Remote Sensing*, *43*(9), 2008–2017. http://dx.doi.org/10.1109/TGRS.2005.853718.

Williams, M., Malhi, Y., Nobre, A. D., Rastetter, E. B., Grace, J., & Pereira, M. G. P. (1998). Seasonal variation in net carbon exchange and evapotranspiration in a Brazilian rain forest: A modelling analysis. *Plant, Cell and Environment*, *21*(10), 953–968. http://dx.doi.org/10.1046/j.1365-3040.1998.00339.x.

Xu, L., Samanta, A., Costa, M. H., Ganguly, S., Nemani, R. R., & Myneni, R. B. (2011). Widespread decline in greenness of Amazonian vegetation due to the 2010 drought. *Geophysical Research Letters*, *38*(7). http://dx.doi.org/10.1029/2011GL046824 (n/a–n/a).

Zanchi, F. B., Waterloo, M. J., Aguiar, L. J. G., von Randow, C., Kruijt, B., Cardoso, F. L., & Manzi, A. O. (2009,). Estimativa do índice de área foliar (IAF) e biomassa em pastagem no estado de Rondônia, Brasil. *Acta Amazonica*, *39*(2), 335–347. http://dx.doi.org/10.1590/S0044-59672009000200012.

Zelazowski, P., Sayer, A. M., Thomas, G. E., & Grainger, R. G. (2011). Reconciling satellite-derived atmospheric properties with fine-resolution land imagery: Insights for atmospheric correction. *Journal of Geophysical Research*, *116*(D18), D18308. http://dx.doi.org/10.1029/2010JD015488.

Zhang, Y., Tian, Y., Myneni, R. B., Knyazikhin, Y., & Woodcock, C. E. (2002). Assessing the information content of multiangle satellite data for mapping biomes. *Remote Sensing of Environment*, *80*(3), 418–434.